Materials for life sciences

Bioactive bone scaffolds manufactured by 3D printing and sacrificial templating of poly(ε-caprolactone) composites as filler for bone tissue engineering

Xiaohong Chen[1], Yujie Liu[2], Hang Liu[1], Lei Li[1], Yubo Liu[1], Ping Liu[1,*] (iD), and Xinghai Yang[2,*]

[1] *School of Materials Science and Engineering, University of Shanghai for Science and Technology, Shanghai 200093, China*
[2] *Department of Orthorpedic Oncology, Changzheng Hospital, Second Military Medical University, 415 Fengyang Road, Shanghai 200003, China*

ABSTRACT

The structures of a bone scaffold play a role in cell attachment and proliferation. In the present work, a poly(ε-caprolactone)/hydroxyapatite/simvastatin (PCL/HA/SIM) composite with a three-dimensional (3D) hierarchical porous structure was successfully fabricated by 3D printing a polyvinyl alcohol (PVA) sacrificial template and a subsequent polymer coating step. The SEM images show that an increase in HA content in the composite significantly decreases the diameter of micropores on the composite surface. The compressive strength measurement results of the composite scaffold show that the strength of the composite scaffold is significantly superior to that of the pure PCL scaffold. Nevertheless, the enhancement of strength in the composite scaffold is not monotonous with more content of HA in the composite as the maximum strength happens for 27.3 wt% of HA. Mouse embryonic fibroblasts (3T3) cells were in vitro cultivated in pure PCL and the composites and demonstrated that more HA content facilitates the proliferation of such cells. Furthermore, an addition of 0.2 wt% of simvastatin (SIM) to the PCL/HA composite scaffold to prepare significantly promoted the proliferation and osteogenic gene expression. The present work shows a potential novel strategy to construct bone tissue engineering scaffolds and cure bone defects.

Xiaohong Chen and Yujie Liu contributed equally to this work.

Address correspondence to E-mail: Pingliu_paper@163.com; cnspineyang@163.com

Introduction

The aim of tissue engineering (TE) is to employ the principles of engineering and life sciences for the development of biological substitutes to repair damaged tissues and restore tissue function [1]. Biomaterials, cells and growth factors are three main factors to apply tissue engineering technology. The function of biomaterials is to construct TE scaffolds for cell growth [2]. Specifically, TE scaffolds for bone tissue regeneration have many distinct requirements, including appropriate mechanical properties, an optimized geometric porous shape with excellent osteogenic activity optimal porosity, pore size and interconnectivity [3]. As such, it is necessary to choose appropriate manufacturing strategies and biomaterial categories (such as natural or synthetic polymers, bioceramics, bioglass, etc.) [4–9].

Polycaprolactone (PCL) is one synthetic polymeric material. Owing to its biodegradable and non-toxic properties, it has been widely used to fabricate bone scaffolds [6, 7]. However, pure PCL has poor cell adhesion ability due to its limited inherent properties [6–9], which could be overcome by combining PCL with other materials [6, 7, 9–11]. For example, it has been reported that hydroxyapatite (HA) was added in to PCL with appropriate concentration. HA significantly enhanced the cell adhesion and differentiation on the surface of PCL, as well as the strength of the PCL composite scaffold [6, 7, 10]. Furthermore, simvastatin (SIM) may be used to modify PCL scaffold. SIM belongs to the class of statin drugs. Many studies regarding in vitro and in vivo experiments of SIM demonstrate its function to facilitate the growth factor expression, especially for VEGF and BMP2, which are two principal regulators of angiogenesis and osteogenesis, respectively. It is promising to fabricate bone TE scaffolds through the combination of biomaterial with SIM to enhance the bone repair success rate and shorten the bone restoration period [12–14].

Fused deposition manufacturing (FDM) is a rapid manufacturing technology, which has been used to manufacture TE scaffolds [10, 15, 16]. In a traditional FDM manufacturing process, thermoplastic material in a melting chamber is extruded from a heated metal nozzle. The nozzle can be shifted horizontally and vertically upon the order from a computer-aided manufacturing software so that the extruded material can be placed on the substrate layer by layer to form a custom designed structure. However, the fine microstructures of the directly printed scaffolds normally need further improvements in order to obtain an efficient bone restoration. In addition, indirect 3D printing techniques of FDM are developed to use sugar complex, polyvinyl alcohol (PVA) or other materials as sacrificial templates. In this way, FDM is enabled to combine other techniques to fabricated complex composition and structures, which significantly promoted cell adhesion and growth in bone TE scaffolds [7, 17–19].

In the present work, indirect 3D printing strategy was used to construct PCL/HA composite scaffolds, which have 3D porous networks. Specifically, polyvinyl alcohol (PVA) was employed as a sacrificial template to complete polymer coating in this strategy. The content of HA has an obvious effect on the mechanical and biological properties. The loaded SIM in the composite scaffold can be slow in vitro released. Mouse embryonic fibroblasts (3T3) have successfully inoculated on the scaffold and in vitro cultured on the scaffold. The proliferation performance of 3T3 and the differentiation of the bone cells are greatly stimulated by the SIM drugs in the scaffold. This strategy is simple, convenient, low cost and easy to combine with other techniques. It has potential applications in the treatment and repair of bone defects.

Materials and methods

Materials

Commercial polyvinyl alcohol (PVA) and medical-grade polycaprolactone (PCL, $M_W = 80,000$) were purchased from Sigma-Aldrich, Co, Ltd.(Milwaukee WI, USA). Hydroxyapatite (HA) and simvastatin (SIM) were obtained from Sinopharm Chemical Reagent Co, Ltd. (Shanghai, China).

Scaffold fabrication

Design and 3D printing of sacrifice template

The sacrificial template of PVA was designed in a size of $20 \times 20 \times 10$ mm using Solidworks®. PVA was loaded on the 3D printer device (Magic Maker Co., China) with a nozzle diameter of 0.4 mm and 3D

Table 1 Material composition and the name of scaffolds

Blend composition	Component quality(g)			Solvent volume (ml)	Scaffold name
	PCL	HA	SIM		
PCL	1.6	0	0	20	PCL
PCL/HA	1.6	0.2	0	20	PCL/HA-1
PCL/HA	1.6	0.6	0	20	PCL/HA-2
PCL/HA	1.6	1.0	0	20	PCL/HA-3
PCL/HA/SIM	1.6	0.6	0.006	20	PCL/HA/SIM-1
PCL/HA/SIM	1.6	0.6	0.012	20	PCL/HA/SIM-2
PCL/HA/SIM	1.6	0.6	0.018	20	PCL/HA/SIM-3

printed through a nozzle at a temperature of 180 °C at a printing speed of 3600 mm/s to result in an internal filling rate of 30%.

Immersion of the template into the mixed solution

The typical protocol of template into the mixed solution is as below: PCL particles were put in in dichloromethane and magnetically stirred at room temperature for 2 h to obtain a transparent solution. Then, HA powders were added into the PCL solution and magnetically stirred to form a homogeneous stable suspension. Thereafter, the sacrificial template of PVA was totally immersed in the suspension for 1 min and air-dried at room temperature in the fume cupboard for 5 min. Similarly, a series of scaffolds were prepared by using different components in dichloromethane to form a series of composite suspension. The data of the corresponding scaffolds prepared in the present work are listed and termed in Table 1 according to mass ratios among the components in the suspension.

Template removal

The as-prepared scaffold was soaked in deionized water and magnetically stirred to remove PVA from the sacrificial template. After a complete dissolution of PVA in the deionized water, the scaffold was put in a vacuum desiccator box at 50 °C. Figure 1 shows the procedure of manufacturing the scaffolds.

Characterization of scaffolds

SEM

The scaffolds were measured by field-emission scanning electron microscopy (FEI QUANTA 450 FEC). The pore diameter, surface morphology and microscopic surface of the scaffold were investigated. Furthermore, the aperture information of the scaffold surface was studied by ImageJ® based on the SEM images.

Porosity

The porosity (%) of the scaffold can be calculated by Eq. 1:

$$\text{Porosity}(\%) = \left(1 - \frac{\text{apparent density of bone scaffold}}{\text{body density of the scaffold}}\right) \times 100\%$$

(1)

Assuming a cuboid shape of the scaffold, the apparent density is calculated by the ratio of weight/volume of the scaffold while the bulk density of the scaffold (PCL:1.145 g cm^{-3}, HA:3.16 g cm^{-3}, SIM:1.11 g cm^{-3}) can be obtained by using a simple mixing rule [20].

Compression test

The mechanical properties of the scaffolds were tested. The compression test of the scaffolds was carried out by using Zwick/Roell Z2.5 (Ennepeta, NRW, Germany) material universal testing machine. The sample has a size of 20 × 20 × 10 mm. The scaffold was compressed at a compression speed of 1 mm/mm till a 80% deformation was obtained. The stress–strain diagram of each scaffold is presented in Figure 4a. The compression modulus E of the bracket can be calculated by fitting the elastic deformation stage. The test was repeated three times for each group.

Figure 1 Schematic diagram of the preparation process of the scaffold.
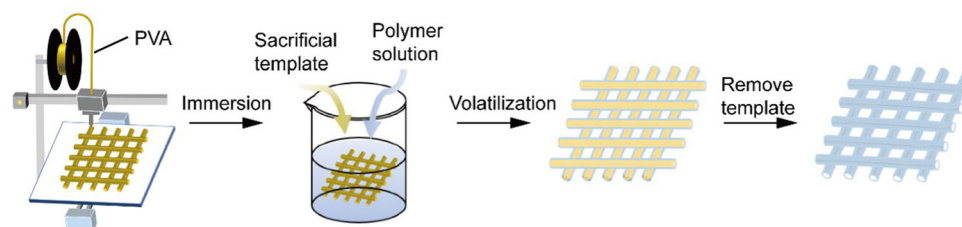
XRD

The phase composition of pure HA, pure PCL, SIM and their composite scaffolds was studied on the X-ray diffractometer (Bruker D8Advance, USA). The measurements were carried out at a scanning speed of 5°/ min from 20 to 60°.

TGA

The thermal stability of the PCL/HA composite scaffolds was studied in the TG/DSC mode using a TGA equipment (STA 449F3, NETZCH company, Germany). 10 mg of the scaffold was placed in the Al2O3 crucible of the TGA equipment. The temperature was raised from 25 to 600 °C at a heating rate of 20 °C/min.

Fourier transform infrared spectrometry (FTIR)

The scaffolds were measured at ambient temperature by LAMBDA750 Fourier transform infrared spectrometer (PerkinElmer, USA) to analyze the functional groups in the samples. FTIR spectra were collected for samples in a wavenumber range of 400-4000 cm^{-1}.

Drug release

SIM was in vitro loaded in the PCL/HA scaffolds. The scaffolds were put in 50 ml PBS buffer and maintained at 37 °C in a thermostatic water bath at a shaking rate of 100 rpm. The PBS buffer was exchanged by a new one every two days. The standard absorbance/concentration calibration curve was collected with Lambda 750UV-visible spectrophotometer (PerkinElmer, USA) at 238 nm wavelength to demonstrate the in vitro release performance of SIM. The remains of SIM in the scaffold were dissolved using dichloromethane and analyzed through an ultraviolet spectrophotometer [21, 22]. The

cumulative release percentage of SIM (%) can be calculated by Eq. 2:

$$SIM(\%) = \frac{\text{released amount at each time point}}{\text{loaded total SIM}} \times 100 \quad (2)$$

where the total amount of loaded SIM is the sum of the release and the final residual release at the last time point of the experiment.

In vitro cell responses on the scaffolds

The as-prepared PCL/HA scaffolds were sterilized in 75% (v/v) ethanol under ultraviolet light irradiation. 3T3 cells were seeded on the scaffolds with a density of 1×10^5 cells/mL and placed in a solution of 10% fetal bovine serum and 1% antibiotic in the 48-well plate. The PCL/HA scaffolds were incubated at 37 °C under an atmosphere with 5% CO_2 concentration. The medium was changed to a new one every two days.

Cell proliferation was measured using a CCK-8 Kit (Cell Counting Kit-8, Beyotime, Shanghai, China). CCK-8 was adjusted to a concentration of 0.5 mg·ml^{-1} and incubated at 37 °C for 4 h. Using a microplate reader (EL800, Bio-Tek Instruments, Winooski, VT, USA), the absorbance at 450 nm was determined (n = 5).

3T3 cell nuclei in the scaffolds were stained using 4′,6-diamidino-2-phenylindole (DAPI) (Thermo Fisher Scientific, Waltham, Massachusetts, USA) in addition to stain the cytoskeleton in FITC Phalloidin (CA1620, Solarbio, Beijing, China). The stained cells were investigated using a confocal microscope (LSM 700, Carl Zeiss, Germany). 3T3 cells were seeded on the PCL/HA scaffold at the same density and cultured for 3 days before the scaffolds were fixed in 2.5% glutaraldehyde. Dehydration of the scaffolds was conducted by a 30 min incubation in a series of ethanol solutions with an increasing concentrations (10, 30, 50, 70, 90, 100%) before hexamethyldisilazane was used for the final dehydration. Being sputter-coated with gold, the PCL/HA scaffolds were

Table 2 Primers in q-PCR analysis

	Forward primers	Reverse primers
OC	5'-CCCTCCTGAAGGTCTCACAA-3'	5'GCTGTCTCCCTCATGTGTTG-3'
OPN	5'-GGAGGAAACCAGCCAAGG-3'	5'-TGCCAGAATCAGTCACTTTCAC-3'
Col-I	5'-ACTCAGCCGTCTGTGCCTCA-3'	5'-GGAGGCCTCGGTGGACATTA-3'
ALP	5'-GCCCAGTGCCTTCTGATTT-3'	5'-GGGCAGCGTCAGATGTTAAT-3'
VEGF	5'-ATGGACGTCTACCAGCGCAGC-3'	5'-CTGCTATGCTGCAGGAAGCTC-3'

measured by SEM to study the adhesion and morphology of 3T3 cells on the PCL/HA scaffolds.

The relative expression of collagen-I (Col-I), osteocalcin (OCN), alkaline phosphatase (ALP), osteopontin (OPN) and vascular endothelial growth factor (VEGF) was measured using real-time quantitative polymerase chain reaction (qPCR), respectively. The total RNA was extracted from cultured scaffolds using the TRIzol reagent (Sigma-Aldrich, Milwaukee, WI, US). Complementary DNA (cDNA) was synthesized from the total RNA. The detailed information of the specific primers for collagen-I (Col-I), osteocalcin (OCN), alkaline phosphatase (ALP), osteopontin (OPN) and vascular endothelial growth factor (VEGF) is listed in Table 2 [20].

Statistical analysis

The same measurements of each sample were repeated 3 times in each experiment. A Student's t test or one-way ANOVA was performed using SPSS software (version 19.0, Chicago, Illinois). P-value < 0.05 was considered to be statistically significant as indicated by different letters in the figures.

Results and discussion

Fabrication and microstructural characterization

Figure 2 shows that the overall structure of the PCL/HA scaffold is ordered and consistent with the shape of the PVA template. After the dissolution of the PVA template, the fibers of the scaffold formed an interconnected tubular stack structure horizontally and vertically through the interlayer intersections as shown in Fig. 2b and f. Furthermore, micropores were generated and evenly distributed over the inner channel wall (Fig. 2d, h) once the solvent evaporated [17], which obviously can facilitate the phase separation mechanism [17] and the exchange of

substances through the walls of the channels to support long-distance material transport. The interconnection between two intersect channels in a scaffold is difficult to obtain according to previously reports [23–25]. The present work demonstrates an efficient strategy to form interconnected microchannels over the fibers of the scaffold, thereby improving physiologically related perfusion to simulate microvessels and facilitate material exchanges in bone restoration (Fig. S1).

Figure 3a to d presents typical SEM images of the pure PCL, PCL/HA-1, PCL/HA-2 and PCL/HA-3 scaffolds. Figure 3a shows micropores with a pore diameter of 1.85 ± 0.29 μm are evenly distributed over the surface of the pure PCL scaffold. Figure 3b shows the pores have an enlarged diameter of 4.46 ± 0.65 μm when HA is added to the scaffolds. However, the diameter of micropores decreases with more HA content. Compared with pure PCL solution, the addition of HA will induce PCL to gather around HA, forming PCL-rich regions, and then reduce the concentration of PCL in other adjacent regions, forming PCL-poor regions, resulting in the increase in pore sizes. The diameters of micropores on the surface of the PCL/HA-3 scaffold cannot be measured due to abundant HA on the surface (38.5 wt%). More HA will increase the viscosity of the printing ink to hinder the formation of micropores in the phase separation process and aggravate the agglomeration of HA [17].
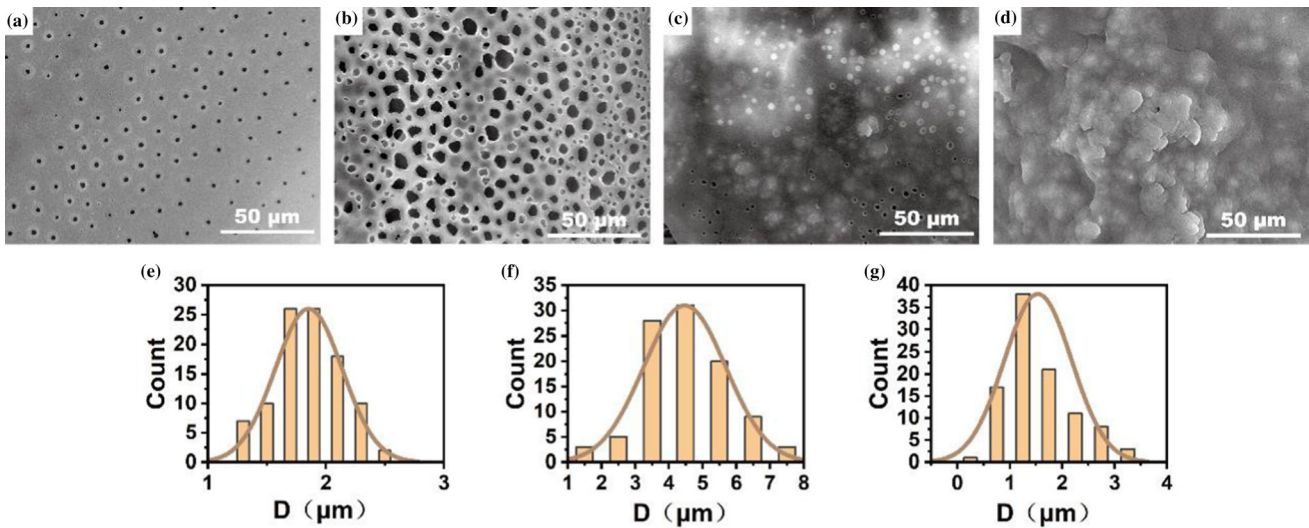
Porosity

Porosity of the scaffolds is displayed in Table 3. The values of porosity for PCL, PCL/HA-1, PCL/HA-2 and PCL/HA-3 scaffolds are $96.94\% \pm 0.51\%$, $96.14\% \pm 0.55\%$, $95.94 \pm 0.52\%$ and $95.13\% \pm 0.45\%$, respectively, all higher than the previously reported data [7, 20]. It is obvious that the porosity decreases with more HA content, which is affected by the composition of the composite [7, 20, 26]. PCL has a
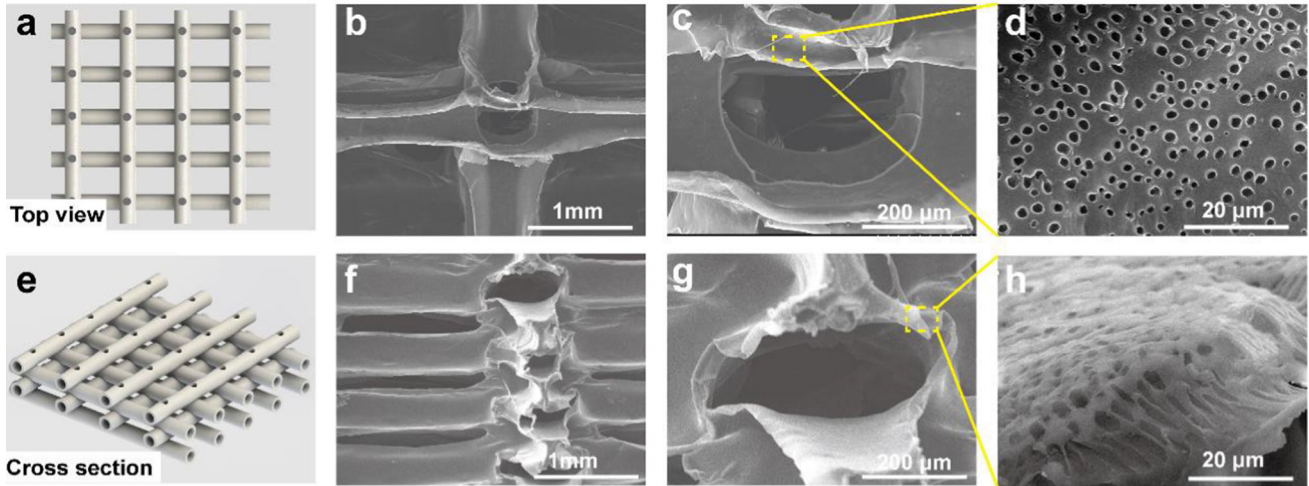
Figure 2 Diagram of scaffold top view (**a**) and SEM (**b-d**). Cross-sectional diagrams (**e**) and SEM (**f-h**).

Figure 3 SEM images of the surface of the scaffolds showing different morphologies: **a** Pure PCL, **b** PCL/HA-1, **c** PCL/HA-2, **d** PCL/HA-3. Pore diameter distribution on the surface of the support: **e** pure PCL, **f** PCL/HA-1, **g** PCL/HA-2.

**Table 3** Surface void size and porosity of scaffolds

	Pore diameter (μm)	Porosity(%)
PCL	1.85 ± 0.29	96.94 ± 0.51
PCL/HA-1	4.46 ± 0.65	96.14 ± 0.55
PCL/HA-2	1.54 ± 0.64	95.94 ± 0.52
PCL/HA-3	-	95.13 ± 0.45

lower density of 1.145 g cm^{-3} than that of HA (3.16 g cm^{-3}). Higher HA content results in lower porosity due to covered surface.

Compression test

Figure 4a presents the stress–strain curves of PCL, PCL/HA-8/1, PCL/HA-8/3 and PCL/HA-8/5, respectively. All the prepared scaffolds exhibits a elastic deformation and scaffold densification process as shown in Fig. 4(a). PCL and HA have significant mechanical properties. PCL shows substantial elasticity, while HA is very brittle at room temperature. Adjustments of the PCL and HA content in the composite scaffold can significantly enhance its mechanical strength. Figure 4a and b indicates that both the compressive strength and modulus of the scaffold are increased by more HA content.

Figure 4 **a** Stress–strain diagram and **b** Compressive modulus for PCL, PCL/HA-1, PCL/HA-2, PCL/HA-3 scaffolds. ((*) indicates significant differences between groups ($p < 0.05$)).
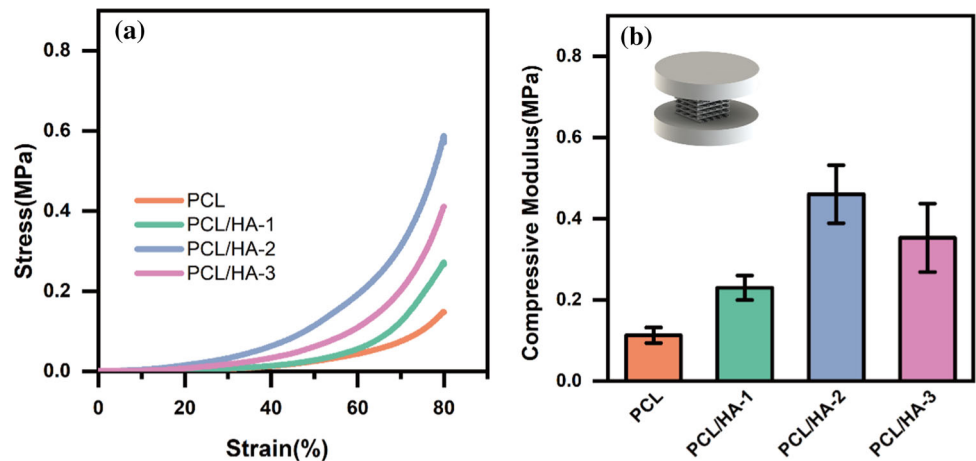
Nevertheless, the maximum compressive strength and compression modulus of the scaffold happened when the proportion of HA reaches 38.5 wt%. This is caused by the agglomeration of HA in the polymer matrix when the content of inorganic fillers in the scaffold above a certain amount. Specifically, the brittleness of HA may impair the reinforcement effect of the composite if it is added too much into the scaffold [6, 10].

Furthermore, the function of the drug release of the PCL/HA scaffold was investigated by loading SIM onto the PCL/HA-2 one. Specifically, a series of samples with SIM at 0.2, 0.4 and 0.8wt% of the total mass of PCL and HA were prepared and termed as PCL/HA/SIM-1, PCL/HA/SIM-2 and PCL/HA/SIM-3, respectively [12, 13] Each scaffold was seeded by the same number of cells and measure cell activity three days later. The PCL/HA/SIM-2 scaffold displayed the highest cell activity (Fig. S3). As such, the PCL/HA/SIM-2 scaffold was chosen for further experiments.

FTIR

FTIR spectra of HA, SIM, the PCL, PCL/HA-2 and PCL/HA/SIM-2 scaffolds are collected and presented in Fig. 5(a). The peaks located at 2940 cm^{-1} in the PCL IR spectrum correspond to the symmetrical stretching vibration of CH$_2$ and its asymmetric stretching vibration at 2860 cm^{-1}, respectively. The peaks at 1720 and 1160 cm^{-1} are assigned to the stretching vibrations of carbonyl groups and C = O [7], respectively. The peaks at 1036 and 3500 cm^{-1} in the HA spectrum are assigned to the PO4^{-3} stretching vibration and the OH stretching vibration [7],

respectively. Multiple peaks spanning over a range of 1300–1000 cm^{-1} in the SIM spectrum are assigned to the C–O–C stretching vibration in the ester groups. The peaks at 1466 and 1384 cm^{-1} are assigned to the C–C angular vibration of the methyl group and the methylene group in the molecule [27, 28]. By comparing the IR spectra of the PCL, PCL/HA-2 and PCL/HA/SIM-2 scaffolds, it is indicated that HA and SIM had a good compatibility with PCL.

XRD

The XRD patterns of pure PCL, PCL/HA-2 and PCL/HA/SIM-2 scaffolds are presented in Fig. 5 (b). In the XRD pattern of the pure PCL scaffold, the strong diffraction peaks at 2θ = 21.3° and 23.8° are assigned to the (110) and (200) crystal planes of PCL, respectively [6, 7]. Two peaks of the PCL/HA-2 scaffold at 2θ = 31.8° and 33° correspond to the (211) and (300) crystal planes of hydroxyapatite [6, 7]. The peak at 2θ = 24.6° in the PCL/HA/SIM-2 XRD pattern is attributed to the SIM component in the PCL/HA/SIM-2 scaffold [27, 28].

TGA

TGA was performed to determine the content of hydroxyapatite loaded on the composite scaffold. As shown in the Fig. 6a, pure PCL decomposed completely at 450 °C [20, 26]. SIM began to decompose at approximately 270 °C and completely at 420 °C. The remains of PCL/HA/SIM-2 and PCL/HA-2 were approximately 26.9 and 27.1 wt%, respectively, which were similar to the loading of HA (27.3%). This indicates PCL and SIM decomposed totally at 450 °C.
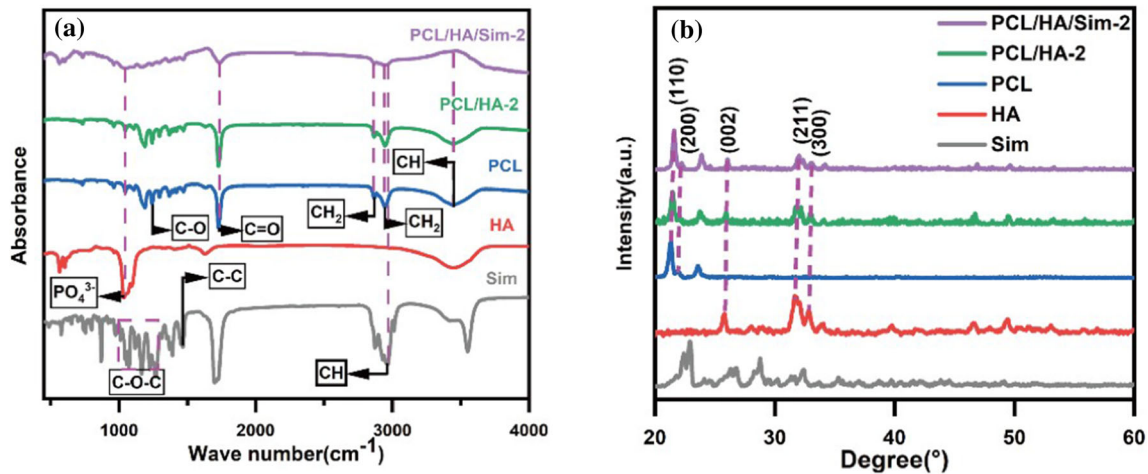
Figure 5 a Fourier transform infrared spectra and **b** XRD for pure SIM, pure HA, pure PCL, PCL/HA-2 and PCL/HA/SIM scaffolds.

Figure 6 a TGA test, **b** the cumulative release of SIM in PCL/HA/SIM-2 scaffold over time.
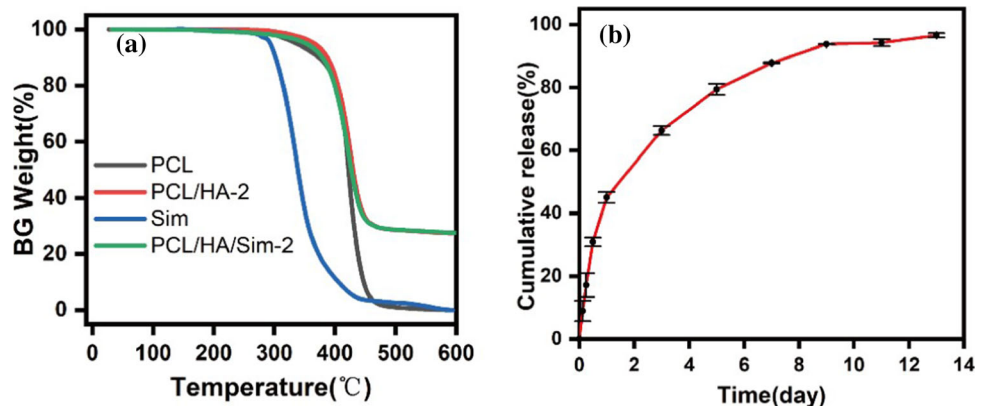
Drug release

The slow release of SIM was studied by a thermostatic shaker for 14 days. The results are shown by the curve in Fig. 6b. SIM was released quickly in the first day by 45.13% of the loaded drug. Then the PCL/HA/SIM scaffold released SIM much slower until the ninth day when the curve of the drug release turn to a plateau. Thereafter SIM hardly releases from the scaffold and approximately 96.57% of SIM was released in the 14 days.
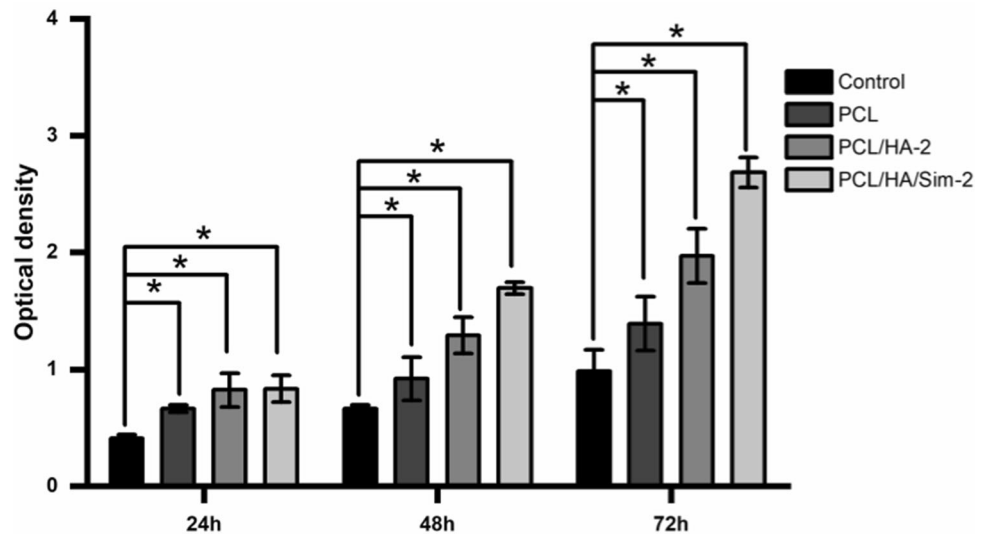
Cell culture

3T3 cells were seeded on the pure PCL, PCL/HA-2 and PCL/HA/SIM-2 scaffolds, respectively, prepared from the sacrificial templates. In addition, one control group of pure PCL sacrificial template was prepared by a direct printing method and termed as control for 3T3 cells seeding. Figure 7 presents the results of the cell viability test by 24, 48 and 72 h. After 24-h cultivation, more cells grow on the as-prepared PCL/HA scaffolds than the control group ($p < 0.05$). The same results were found after 48- and 72-h cultivation although the cell activities in all measured groups increase significantly and the number of living cells in all groups was statistically similar ($p < 0.05$). It is shown that the 3D indirect printing strategy can provide an environment superior to the one from direct 3D printing method for the growth of cells. Additionally, both HA and SIM can play an active role in cell metabolism. As such, 3T3 cells on the PCL/HA-2 and PCL/HA/SIM-2 scaffolds exhibit more efficient growth activities than the pure PCL scaffolds in the whole cultivation period. Specifically, the PCL/HA/SIM-2 scaffolds exhibit

Figure 7 The results of cell viability test of scaffolds after 24,48,72 h. ((*) indicates significant differences between groups ($p < 0.05$)).

Figure 8 3-day culture of 3T3 cells, the DAPI (**a-d**), FITC (**e–h**) fluorescence images and SEM (**i-l**) of the control group (traditional scaffolds), PCL, PCL/HA-2 and PCL/HA/SIM-2 composite scaffolds.
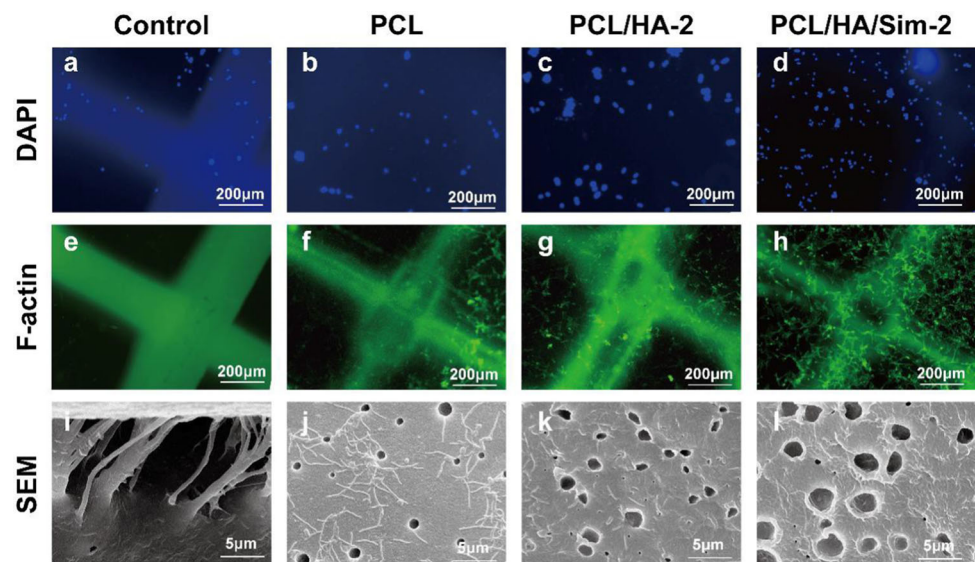

higher cellular activities than the PCL/HA-2 scaffolds at 48- and 72-h measurements, respectively.

After the 3-day culture process, the PCL/HA scaffolds were stained and measured by SEM. Figure 8a to d presents 3T3 images of control, pure PCL, PCL/HA-2 and PCL/HA/SIM-2 scaffolds. The number of 3T3 cells stained with DAPI was consistent with the results of the cell viability assay [20]. Figure 8e to h presents 3T3 cells images of control, pure PCL, PCL/HA-2 and PCL/HA/SIM-2 scaffolds stained by FITC, respectively. It is observed that the green fluorescent spots increased gradually at the scaffold fibers intersection zone under the same

culture conditions, indicating more viable cells on the scaffolds than on scaffolds prepared by traditional methods. SEM images in Fig. 8(i) to (l) demonstrate the similar results to the ones from DAPI and FITC. All scaffolds satisfy suitable cell attachment and growth. Nevertheless, the smooth surface of the control weakens the adhesion of 3T3 cells to the scaffold. Only a few of cells are found in the gap between the layers of the scaffold. Much more cells cultured on the PCL, PCL/HA-2 and PCL/HA/SIM-2 scaffolds were observed within the microporous than the cells observed in the control group, indicating the function of the microporous structure to

Figure 9 Osteogenic gene (Col-I, OC, ALP, OPN) and VEGF expression of the pure PCL and composite scaffolds after 7 days of cell culturing. ((*) indicates significant differences between groups ($p < 0.05$)).
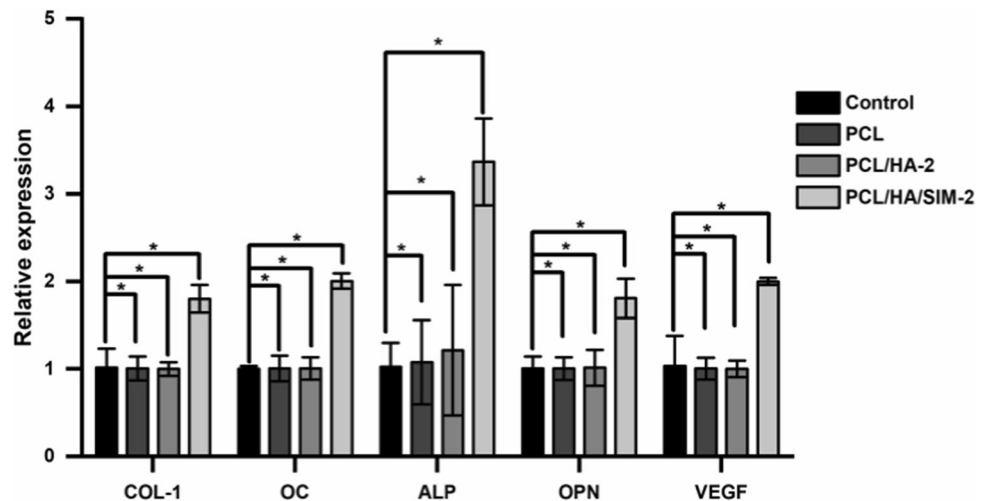
benefit cell attachment [17, 20, 29]. Much more rough surfaces were generated after the addition of HA in the scaffolds, resulting in an increased number of cells on the PCL/HA-2 scaffold. Furthermore, SIM promoted cell proliferation on the PCL/HA/SIM-2 scaffold to the best performance for the scaffolds in the present work.

The osteogenic differentiation of 3T3 cells on each scaffold was evaluated using qPCR to determine the expression levels of Col-I, OC, ALP, OPN and VEGF. Figure 9 presents the relative expression results of the control, PCL, PCL/HA-2 and PCL/HA/SIM-2 scaffolds. Among the four types of scaffolds, 3T3 cells on PCL/HA/SIM-2 exhibited the highest levels of gene expression, indicating the effective performance of SIM in promoting osteogenic differentiation and vascularization of 3T3 cells.

Based on the experimental results in the present work, the drug release mechanism of SIM is proposed as below. Novel bioactive bone scaffolds are firstly fabricated with 3D interconnected pipe networks. The hierarchical porous structure is formed due to phase separation and solvent evaporation. In comparison with the direct printing scaffolds as showing in Fig. 10a, the hierarchical porous structure can provide higher porosity. The microporous on the scaffold surfaces can further connect many large conduits for fast nutrient transfer and discharge of metabolic waste (Fig. 10b). This can provide an excellent environment to stimulate cell growth. The as-prepared composite scaffold can in situ release SIM to further promote the proliferation of CTC3 cells and induct bone differentiation.
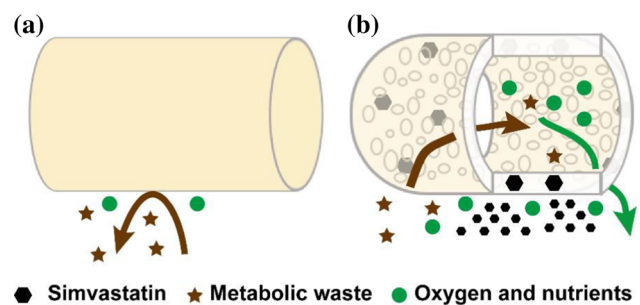
Figure 10 Direct printing prepared scaffold (**a**) and our porous scaffold (**b**) cell culture nutrient metabolism model.

Conclusion

In the present work, PCL/HA/SIM composite scaffolds were successfully prepared using 3D printing with a sacrificial template strategy. The as-prepared scaffolds exhibited a high porosity more than 95% of stacked and interconnected conduits. The hierarchical porous structure provided an excellent environment for bone cell growth. A high content of HA component can reduce the diameter of micropores on the scaffold surfaces. More HA can increase the bioactivity of the composite scaffolds but significantly weaken the strength of the PCL/HA/SIM scaffolds. Furthermore, the PCL/HA/SIM-2 scaffold can release 96.57% of the active drug within 14 days. Specifically, we demonstrated that the PCL/HA/SIM-2 scaffold performed the best mechanical strength and cell activities when 27.3 wt% of HA and 0.4 wt% of SIM content were employed. In summary, the as-prepared PCL/HA/SIM scaffold has a great potential application for bone tissue engineering.

Declarations

Conflict of interest The authors declare that they have no known competing financial interests or personal relationships that could have appeared to influence the work reported in this paper.

Supplementary Information: The online version contains supplementary material available at https://doi.org/10.1007/s10853-023-08319-4.

References

[1] Vacanti JP, Langer R (1999) Tissue engineering: the design and fabrication of living replacement devices for surgical reconstruction and transplantation. Lancet 354:S32–S34. https://doi.org/10.1016/S0140-6736(99)90247-7

[2] Wu Z, Su X, Xu Y et al (2016) Bioprinting three-dimensional cell-laden tissue constructs with controllable degradation. Sci Rep 6:24474. https://doi.org/10.1038/srep24474

[3] Kosik-Kozio A, Graham E, Jaroszewicz J et al (2019) Surface modification of 3D printed polycaprolactone constructs via a solvent treatment: impact on physical and osteogenic properties. ACS Biomater Sci Eng 5:318–328. https://doi.org/10.1021/acsbiomaterials.8b01018

[4] Pilia M, Guda T, Appleford M (2013) Development of composite scaffolds for load-bearing segmental bone defects. BioMed Res Int 1:458253. https://doi.org/10.1155/2013/458253

[5] Middleton JC, Tipton AJ (2000) Synthetic biodegradable polymers as orthopedic devices. Biomaterials 21:2335–2346. https://doi.org/10.1016/S0142-9612(00)00101-0

[6] Kim JY, Lee TJ, Cho DW et al (2010) Solid free-form fabrication-based PCL/HA scaffolds fabricated with a multi-head deposition system for bone tissue engineering. J Biomater Sci Polymer Edition 21:951–962. https://doi.org/10.1163/156856209X458380

[7] Shadi H, Ali K-P, Ahmad O, Tahereh T-Kh (2019) Preparation and characterization of PLA/PCL/HA composite scaffolds using indirect 3D printing for bone tissue engineering. Mater Sci Eng: C 104:109960. https://doi.org/10.1016/j.msec.2019.109960

[8] Heydari Z, Mohebbi-Kalhori D, Afarani MS (2017) Engineered electrospun polycaprolactone (PCL)/octacalcium phosphate (OCP) scaffold for bone tissue engineering. Mater Sci Eng, C 81:127–132. https://doi.org/10.1016/j.msec.2017.07.041

[9] Fonseca GFD, Avelino SDOM, Mello DDCR et al (2020) Scaffolds of PCL combined to bioglass: synthesis, characterization and biological performance. J Mater Sci - Mater Med 13:21–37. https://doi.org/10.24237/djps.1303.189C

[10] Rodenas-Rochina J, Ribelles JLG, Lebourg M (2013) Comparative study of PCL-HAp and PCL- bioglass composite scaffolds for bone tissue engineering. J Mater Sci Mater Med 24:1293–1308. https://doi.org/10.1007/s10856-013-4878-5

[11] Steffen S, Cassan D, Robert H et al (2019) Layer-by-layer deposition of chitosan nanoparticles as drug-release coatings for PCL nanofibers. Biomater Sci 7:233–246. https://doi.org/10.1039/C8BM00657A

[12] Killeen AC, Rakes PA, Schmid MJ et al (2012) Impact of local and systemic alendronate on SIM- induced new bone around periodontal defects. J Periodontol 83:1463–1471. https://doi.org/10.1902/jop.2012.110683

[13] Pullisaar Helen, Tiainen Hanna, Landin Maria A et al (2013) Enhanced in vitro osteoblast differentiation on TiO2 scaffold coated with alginate hydrogel containing SIM. J Tissue Eng. https://doi.org/10.1177/20417314135156

[14] Calixto JC, Villaboim CE, de Castro Lima L, Frederico L et al (2011) The influence of local administration of simvastatin in calvarial bone healing in rats. J Cranio- Maxillofacial Surg 39:215–220. https://doi.org/10.1016/j.jcms.2010.03.009

[15] Lipson H, Kurman M (2013) Fabricated: the new world of 3D printing[M]. Wiley Publishing

[16] Kankala KR, Xiao-Ming M et al (2018) 3D-printing of microfibrous porous scaffolds based on hybrid approaches for bone tissue engineering. Polymers 10:807. https://doi.org/10.3390/polym10070807

[17] Lei D, Yang Y, Liu Z et al (2019) 3D printing of biomimetic vasculature for tissue regeneration. Mater Horiz 6:1197–1206. https://doi.org/10.1039/C9MH00174C

[18] Miller JS, Stevens KR, Yang MT et al (2012) Rapid casting of patterned vascular networks for perfusable engineered three-dimensional tissues. Nat Mater 11:768–774. https://doi.org/10.1038/nmat3357

[19] Bellan LM, Singh SP, Henderson PW et al (2009) Fabrication of an artificial 3-dimensional vascular network using sacrificial sugar structures. Soft Matter 5:1354–1357. https://doi.org/10.1039/B819905A

[20] Kim YB, Lim JY, Yang GH et al (2019) 3D-printed PCL/bioglass (BGS-7) composite scaffolds with high toughness and cell-responses for bone tissue regeneration. J Ind Eng Chem 79:163–171. https://doi.org/10.1016/j.jiec.2019.06.027

[21] Bose S, Sarkar N, Vahabzadeh S (2019) Sustained release of vitamin C from PCL coated TCP induces proliferation and differentiation of osteoblast cells and suppresses

osteosarcoma cell growth. Mater Sci Eng: C 105:110096. https://doi.org/10.1016/j.msec.2019.110096

[22] Moshiri A, Shekarchi B, Oryan A et al (2015) Three-dimensional porous Gelapin–simvastatin scaffolds promoted bone defect healing in rabbits. Calcif Tissue Int 96:552–564. https://doi.org/10.1007/s00223-015-9981-9

[23] Zhang Y, Yu Y, Chen H et al (2013) Characterization of printable cellular micro-fluidic channels for tissue engineering. Biofabrication. https://doi.org/10.1088/1758-5082/5/2/025004

[24] Zhang Y, Yu Y et al (2013) Direct bioprinting of vessel-like tubular microfluidic channels. J Nanotechnol Eng Med 4:020902. https://doi.org/10.1115/1.4024398

[25] Yu Y, Zhang Y, Martin JA et al (2013) Evaluation of cell viability and functionality in vessel-like bioprintable cell-laden tubular channels. J Biomech Eng 135:091011. https://doi.org/10.1115/1.4024575

[26] Swietek M, Broz A, Tarasiuk J et al (2019) Carbon nanotube/iron oxide hybrid particles and their PCL-based 3D composites for potential bone regeneration. Mater Sci Eng 104:109913. https://doi.org/10.1016/j.msec.2019.109913

[27] Liu C, Liu H, Chen L et al (2005) Spectral data analysis and identification of simvastatin. Anal Chem 33(007):985–988. https://doi.org/10.1038/sj.cr.7290370

[28] Zhang J, Shen Z, Chen J (2005) Preparation of micronized simvastatin by freeze-drying of hydrosol. J Chem Eng Chin Univ 20(005):814–819. https://doi.org/10.1016/j.morpho.2007.09.079

[29] Jinbing W, Dingyu W, Zhanzhao Z et al (2015) Biomimetically ornamented rapid prototyping fabrication of an apatite-collagen-polycaprolactone composite construct with nano-micro- macro hierarchical structure for large bone defect treatment. ACS Appl Mater Interfaces 7:26244–26256. https://doi.org/10.1021/acsami.5b08534